Journal of Materials Science: Materials in Electronics (2019) 30:17999–18014
https://doi.org/10.1007/s10854-019-02153-8

Microstructural, optical and electrochromical properties of W-doped Nb_2O_5 thin films prepared by dip-coating process using sols obtained by the chloroalkoxide route

Anil Kumar[1] · **P. P. Sahay**[1]

Received: 17 July 2019 / Accepted: 3 September 2019 / Published online: 9 September 2019

Abstract
Undoped and W-doped Nb_2O_5 thin films have been characterized by X-ray diffraction (XRD), scanning electron microscopy (SEM) and atomic force microscopy (AFM) in order to study the influence of W doping on their structural and morphological properties. The synthesized Nb_2O_5 thin films have been found to possess an orthorhombic crystal structure having crystallite sizes 10–31 nm. The UV–visible spectroscopy shows the optical bandgap ~ 3.60 eV. The cyclic voltammetric studies show that the colouration efficiency of the films improves upon W doping with the optimum value of 68.7 cm^2/C at 600 nm for the 3 at.% W-doped film. The chronoamperometric studies reveal that the switching response of the films becomes better upon W doping. The electrochemical impedance spectroscopy (EIS) data has been analyzed by fitting it to the equivalent electrical circuit (EEC) using Nova software.

1 Introduction

Thin films of niobium pentoxide (Nb_2O_5) are promising candidates for electrochromic device applications such as smart windows, electronic displays and electro-optic devices [1–3]. Among the different stoichiometries of niobium oxide, namely NbO, Nb_2O_3, NbO_2 and Nb_2O_5, niobium pentoxide is thermodynamically stable [4, 5] and has been the focus of much attention to researchers owing to its unique electrochromic properties. It has been found that niobium pentoxide films reversibly and persistently change their colours on applying an external electric potential to them [6, 7]. Colour change arises due to insertion and removal of ions into and out the material during electrochemical redox reactions. In the case of crystalline Nb_2O_5 films, the colour changes from transparent to blue under the influence of applied electric potential, whereas brown colouring effect is observed in the amorphous Nb_2O_5 films [8].

The electrochromic properties of Nb_2O_5 thin films are strongly dependent upon the microstructural features of the films, which can be modified by the addition of appropriate dopants in the host lattice network. Schmitt and Aegerter [9] have studied Zr, Sn, Li, Ti and Mo- doped Nb_2O_5 films prepared by the dip-coating technique. Heusing et al. [10] have examined the influence of Mo and Li doping independently in the electrochromic performance of Nb_2O_5 films and found that the film undergoes a change in colour from transparent to brown, grey or blue depending on the crystallinity of the film. Pehlivan et al. [6] have investigated tantalum pentoxide-doped Nb_2O_5 films prepared by sol–gel spin-coating method. Microstructural and electrochromic characteristics of WO_3-doped Nb_2O_5 thin films have been studied by Pehlivan et al. [11].

The microstructural characteristics of the films are influenced greatly by the film preparation technique as well as preparation conditions including precursors, temperature, etc. Various deposition techniques have been used to prepare Nb_2O_5 films, which include sol–gel spin-coating [6], dip-coating [9–11], RF sputtering [12], spray pyrolysis [13], chemical vapour deposition [14], hydrothermal process [15], etc. Pehlivan et al. [6] have reported amorphous nature of as-deposited 15% Ta_2O_5-doped Nb_2O_5 films employing sol–gel spin-coating technique using niobium (V) ethoxide and tantalum (V) ethoxide as precursors. Schmitt and Aegerter [9] have reported four different structures for the sol–gel derived Nb_2O5:Ti and Nb_2O_5:Mo films, which depend upon the sintering-temperature as well as the doping level. Al-Baradi et al. [12] have found an orthorhombic phase for the

✉ P. P. Sahay
dr_ppsahay@rediffmail.com

[1] Department of Physics, Motilal Nehru National Institute of Technology Allahabad, Prayagraj 211004, India

rf sputtered Nb_2O_5 films. Mujawar et al. [13] have reported a monoclinic phase of Nb_2O_5 for the spray-deposited films. Amorphous nature of the Nb_2O_5 films prepared by the chemical vapour deposition at 350 °C has been reported by Maruyama and Kanagawa [14]. Wen et al. [15] have reported an orthorhombic structure for the hydrothermally synthesized Nb_2O_5 nanorod array films.

Our intent in the present investigation is to study the effect of W doping on the microstructural, optical and electrochromic properties of Nb_2O_5 films prepared by the dip-coating method using sols obtained by the chloroalkoxide route, i.e. by dissolving niobium pentachloride in ethanol and acetic acid. To the best of our knowledge, such study on the influence of W doping in the Nb_2O_5 films has not yet been reported in literatures.

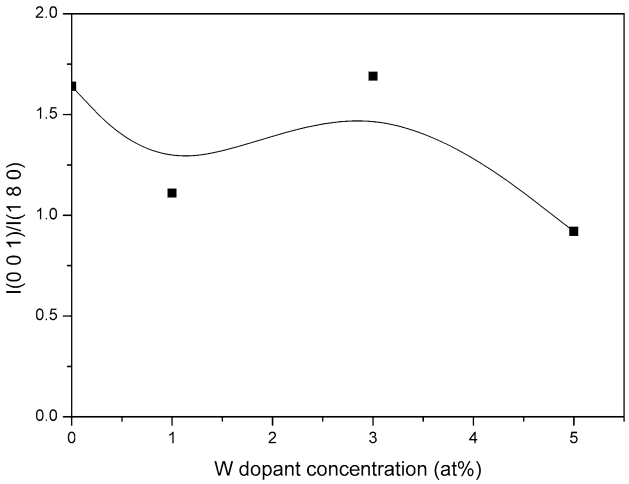

Fig. 2 Intensity ratio $I(0\ 0\ 1)/I(1\ 8\ 0)$ as a function of W dopant concentration

2 Experimental details

All the chemicals used here were of high purity. Firstly, niobium chloroethoxide solution of 0.2 M concentration was prepared by dissolving required amount of $NbCl_5$ in ethanol. Next, required amount of acetic acid (Ac) was added to the solution to get molar ratio Nb:Ac = 1:2. The mixture was then ultrasonicated at room temperature for 30 min. Ultrasonification process accelerates the chemical reaction of $NbCl_5$ with ethanol and acetic acid. The sol of Nb_2O_5 was thus prepared. For W doping, required amount of $(NH_4)_2WO_4$ was first dissolved in a little amount of warm water, and then after cooling it to room temperature, it was added to the above-prepared sol. The thin films of undoped and W-doped Nb_2O_5 were deposited onto the glass and fluorine doped tin oxide (FTO) coated glass substrates by the dip-coating process. Prior to deposition, the glass substrates were thoroughly cleaned, first by labolene detergent and then rinsed with deionized water, and again ultrasonicated in trichloroethylene for 15 min and further rinsed with

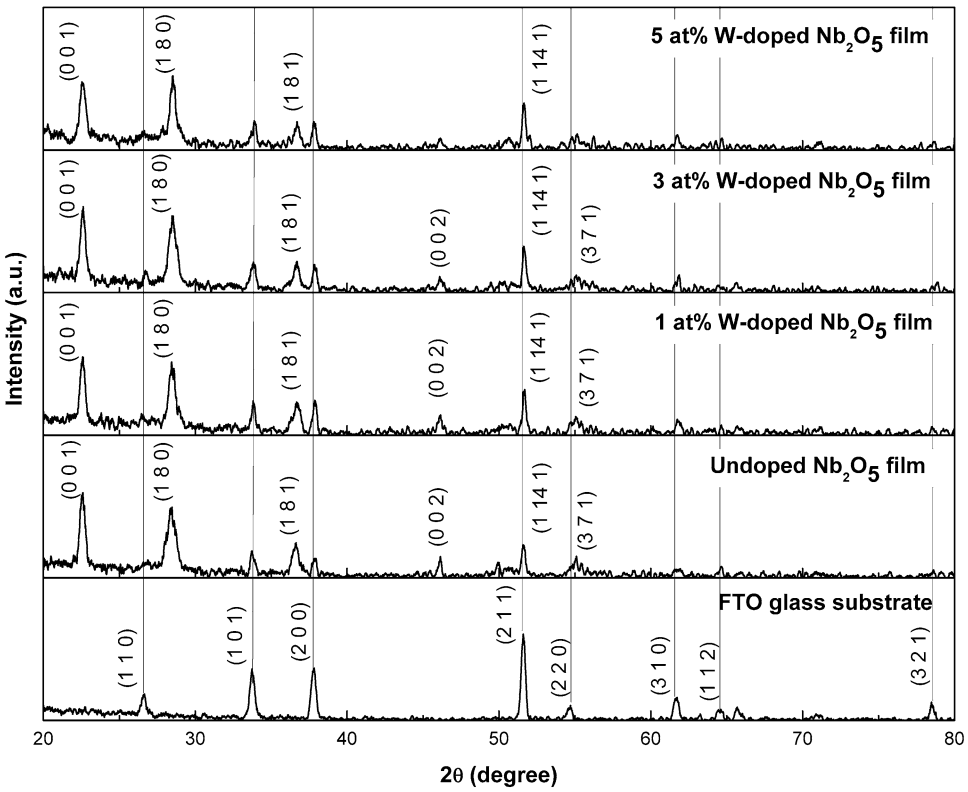

Fig. 1 XRD profiles of the W-doped Nb_2O_5 thin films. Vertical lines correspond to the peaks of FTO glass

Table 1 Structural parameters of undoped and W-doped Nb_2O_5 films

Samples	XRD peaks		Lattice strain	Crystallite size (nm)	Unit cell parameters (Å)	Unit cell volume (Å^3)
	d-spacing (Å)	(hkl)				
Undoped Nb_2O_5 film	3.93781	(0 0 1)	0.0084	21.1	a = 6.062	700.48
	3.1382	(1 8 0)	0.0132	10.7	b = 29.343	
	2.45254	(1 8 1)	0.0076	14.5	c = 3.938	
	1.7696	(1 14 1)	0.0026	30.6	α = β = γ = 90°	
1 at.% W-doped Nb_2O_5 film	3.93424	(0 0 1)	0.0084	21.1	a = 5.968	689.11
	3.12556	(1 8 0)	0.0066	21.3	b = 29.351	
	2.44668	(1 8 1)	0.0101	10.9	c = 3.934	
	1.76722	(1 14 1)	0.0034	23.0	α = β = γ = 90°	
3 at.% W-doped Nb_2O_5 film	3.93122	(0 0 1)	0.0063	28.1	a = 6.106	705.01
	3.13701	(1 8 0)	0.0099	14.2	b = 29.252	
	2.44809	(1 8 1)	0.0101	10.9	c = 3.931	
	1.76616	(1 14 1)	0.0052	15.3	α = β = γ = 90°	
5 at.% W-doped Nb_2O_5 film	3.93606	(0 0 1)	0.0105	16.9	a = 5.941	687.46
	3.12527	(1 8 0)	0.0066	21.3	b = 29.399	
	2.44678	(1 8 1)	0.0076	14.5	c = 3.936	
	1.76871	(1 14 1)	0.0026	30.6	α = β = γ = 90°	

deionized water several times. Finally, the substrates were dried in air at room temperature. After dipping the cleaned substrates into sols for a while, the substrates were gently taken out the sols. The films thus deposited on the substrates were first dried in air at room temperature followed by thermal treatment at 550 °C for 40 min in air. The as-prepared film in each case has the electrode area of 1.5 cm^2.

The post-heat treated films were subjected to further characterizations of microstructural, optical and electrochromical properties. The crystallographic phases of the films were characterized by X-ray diffraction (XRD) using a Rigaku X-ray diffractometer with CuKα_1 ($\lambda = 1.5406$ Å) radiation within the range of 10–80° (2θ) in glancing angle mode. The surface morphologies of the films were examined using a field-emission scanning electron microscope [Model: Nova NanoSEM 450] and a scanning probe microscope [Model: NT-MDT NTEGRA Prima]. Elemental analyses of the films were conducted with an EDS (Energy dispersive X-ray spectroscopy) detector attached to the scanning electron microscope. The UV–visible transmittance spectra of the films were obtained from a Shimadzu UV–Vis–NIR spectrometer [Model: UV 3600 Plus] in the wavelength range 300–800 nm at normal incidence. The electrochromic properties of the films were analysed using an Electrochemical Analyser (Model: Autolab PGSTAT101) controlled by Nova software and a conventional three-electrode electrochemical cell containing a 0.1 M solution of $LiClO_4$ dissolved in propylene carbonate as the electrolyte, Nb_2O_5 film deposited on the FTO glass substrate as the working electrode, a platinum wire as the counter electrode, and Ag/AgCl as the reference-electrode.

3 Results and discussion

3.1 Film formation

Dip-coating process used in the present investigation is a facile and economical technique to deposit thin films on a substrate. The technique involves immersing a substrate into the precursor solution at a constant speed followed by holding it for some time and finally withdrawing the substrate from the solution at a constant speed. The microstructural features of the films are influenced greatly by various process parameters such as immersion time, withdrawal speed, precursor solution concentration, dip-coating cycles, etc. [16, 17]. To prepare Nb_2O_5 thin films, sols were obtained by the chloroalkoxide route. First, on dissolving $NbCl_5$ in ethanol, niobium chloroethoxide is formed by partial alcoholysis [17, 18]:

$$NbCl_5 + xC_2H_5OH \rightarrow NbCl_{(5-x)}\left(OC_2H_5\right)_x + xHCl \quad (1)$$

When acetic acid is added to the solution, it reacts with the excess ethanol forming ethyl acetate and water:

$$CH_3COOH + C_2H_5OH \rightarrow CH_3COOC_2H_5 + H_2O \quad (2)$$

Niobium chloroethoxide already formed in the solution then undergoes both the hydrolysis and condensation reactions, resulting in the formation of Nb_2O_5 sol [19]:

$$NbCl_{(5-x)}\left(OC_2H_5\right)_x + 5H_2O \rightarrow xC_2H_5OH + (5-x)HCl + Nb(OH)_5 \quad (3)$$

$$2Nb(OH)_5 \rightarrow Nb_2O_5 + 5H_2O \quad (4)$$

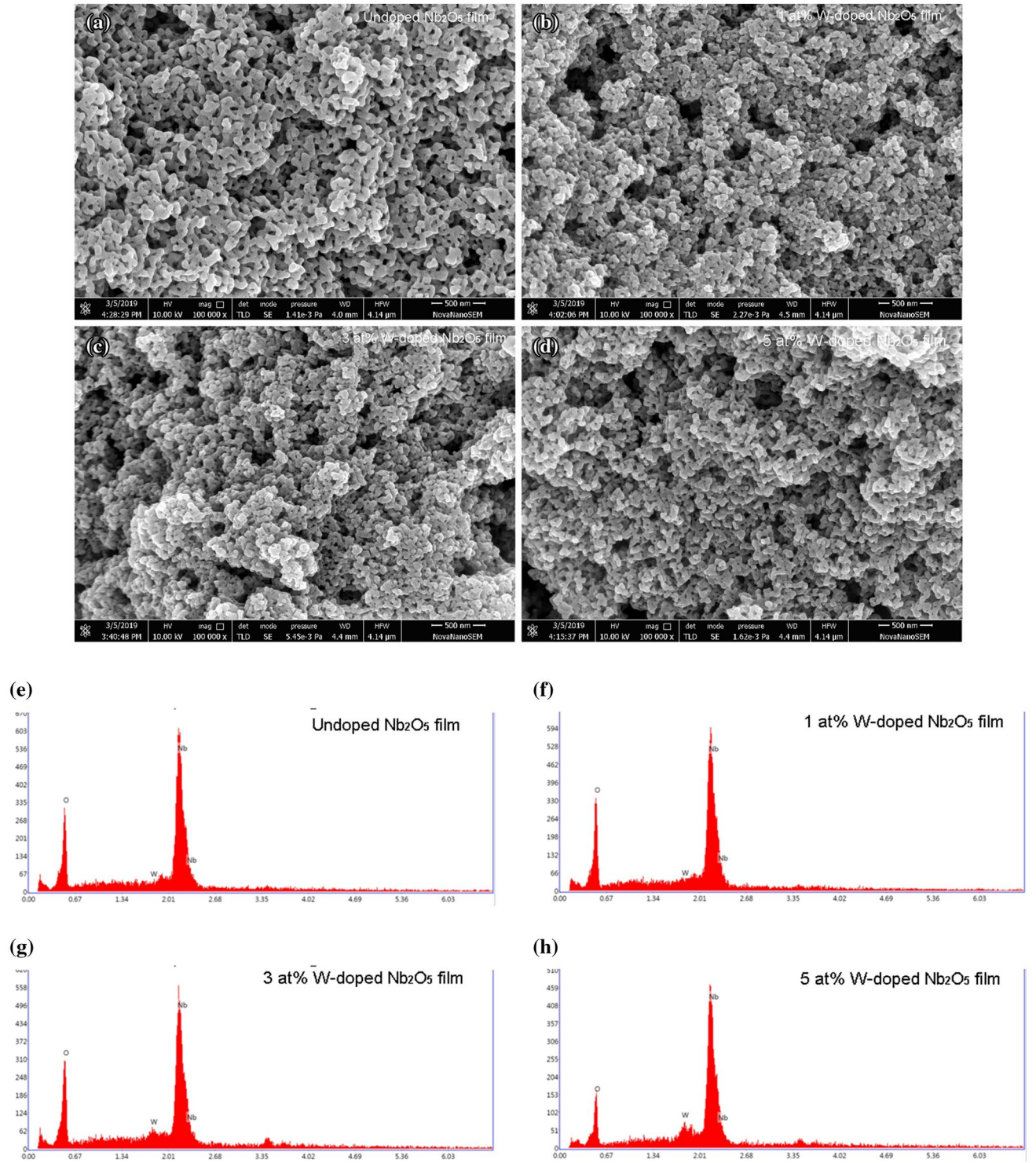

Fig. 3 **a**–**h** FESEM micrographs and the corresponding EDS profiles of the Nb_2O_5 films

3.2 Microstructural studies

X-ray diffraction profiles of the undoped and W-doped Nb_2O_5 thin films deposited on FTO coated glass substrates are depicted in Fig. 1. Analyses of the XRD results using X'Pert HighScore Plus software reveal that the diffraction profiles are in good agreement with the JCPDS card no. 30-0873 and therefore all the films are polycrystalline having

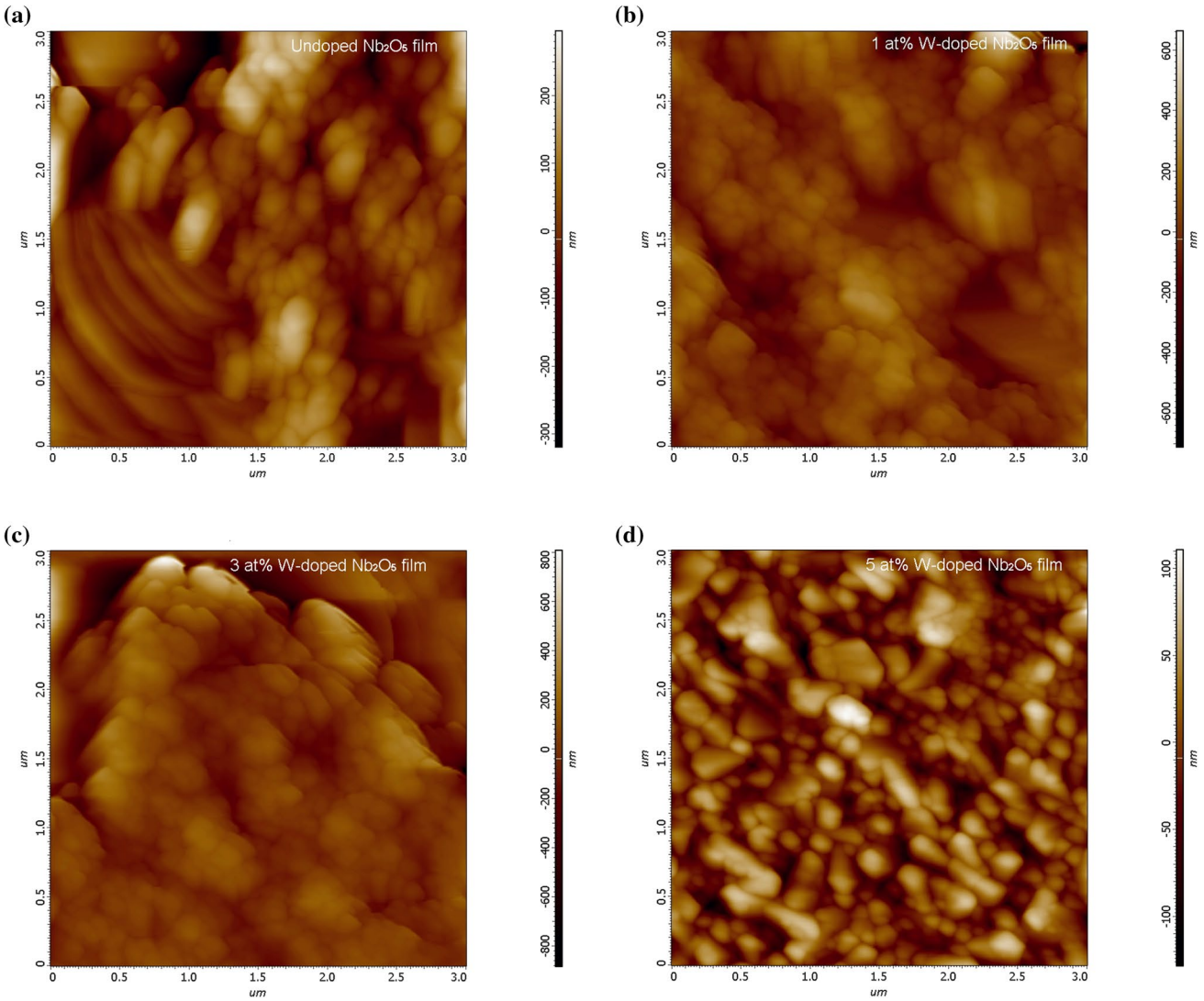

Fig. 4 **a**–**h** Two-dimensional (2D) and three-dimensional (3D) AFM images of the Nb_2O_5 films

an orthorhombic phase of niobium pentoxide. In addition to XRD peaks of FTO glass, prominent peaks corresponding to (0 0 1), (1 8 0), (1 8 1), and (1 14 1) planes of Nb_2O_5 are observed in the patterns. In 5 at.% W-doped film, the most intense peak is (1 8 0) followed by the peak (0 0 1), whereas in all other films, the peak (0 0 1) is the most prominent one followed by the peak (1 8 0). Figure 2 presents a change in the preferential orientation $I(0\ 0\ 1)/I(1\ 8\ 0)$ of the lattice planes with increase in W dopant concentration. The orthorhombic phase of Nb_2O_5 has been reported by other researchers also [6, 8, 20]. Pehlivan et al. [6] have obtained the orthorhombic phase of sol–gel spin-coated Nb_2O_5 thin films when the films were calcined at 550 °C in air for 10 h. Pawlicka et al. [8] have reported the orthorhombic phase of Nb_2O_5 films prepared by the sol–gel method on calcination of the films at around 600 °C. Raba et al. [20] have reported the formation of orthorhombic Nb_2O_5 phase upon heat-treatment of the sol–gel synthesized niobium pentaoxide powders at 750 °C in air.

The unit cell parameters have been determined from the XRD peaks and are listed in Table 1. It has been found that the unit cell parameters for the undoped Nb_2O_5 thin films are very close to the values listed in JCPDS card no. 30-0873 (a = 6.175 Å, b = 29.17 Å, c = 3.930 Å, and angles $\alpha = \beta = \gamma = 90°$). Being the different ionic radii of W^{6+} and Nb^{5+} the incorporation of tungsten ions into Nb_2O_5 lattice system results in a little change in the lattice parameters of the unit cell in the W-doped films. The crystallite size and the lattice strain of the films have been estimated by the Scherrer equation and the tangent formula, respectively.

The two-dimensional (2D) high magnification surface morphological study of the Nb_2O_5 films has been carried

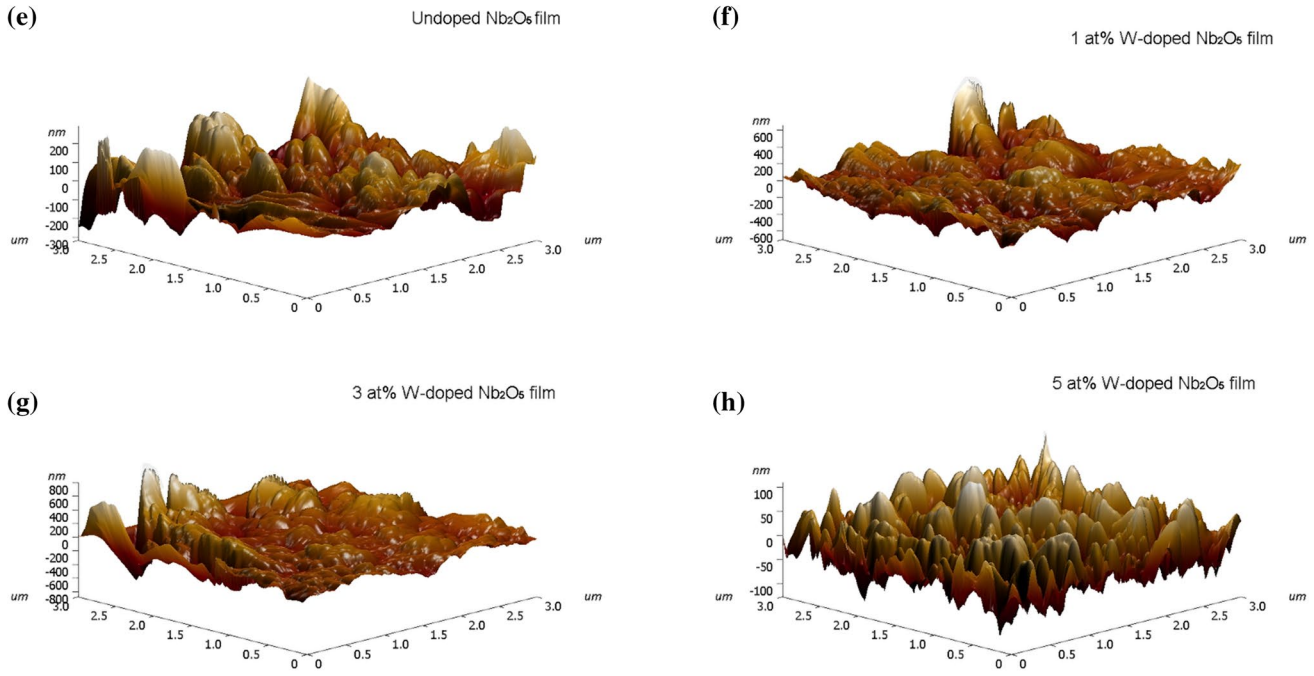

Fig. 4 (continued)

Table 2 Topographical parameters of undoped and W-doped Nb_2O_5 films

Samples	Image surface area (μm^2)	Image projected surface area (μm^2)	Root mean square roughness, R_q (nm)	Average roughness, R_a (nm)
Undoped Nb_2O_5 film	13.884	9.011	77.448	58.157
1 at.% W-doped Nb_2O_5 film	20.544	9.011	106.440	80.874
3 at.% W-doped Nb_2O_5 film	38.872	9.011	134.447	93.287
5 at.% W-doped Nb_2O_5 film	11.907	9.011	34.142	27.570

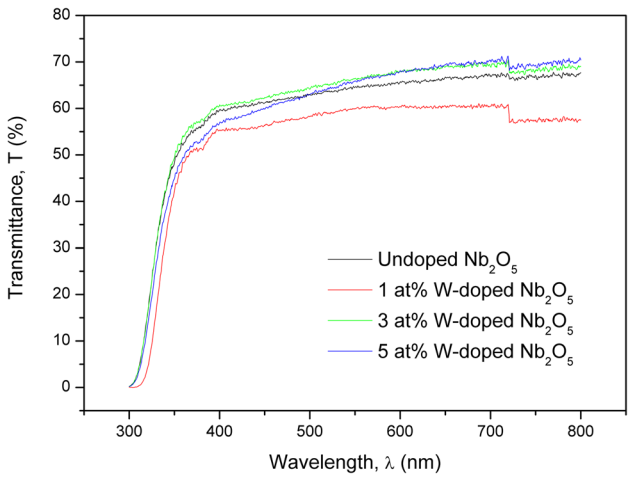

Fig. 5 Transmission spectra of the Nb_2O_5 films

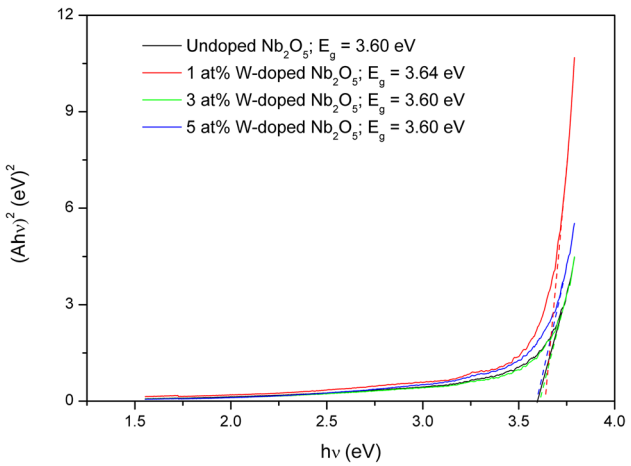

Fig. 6 Plot of $(Ah\nu)^2$ versus $h\nu$

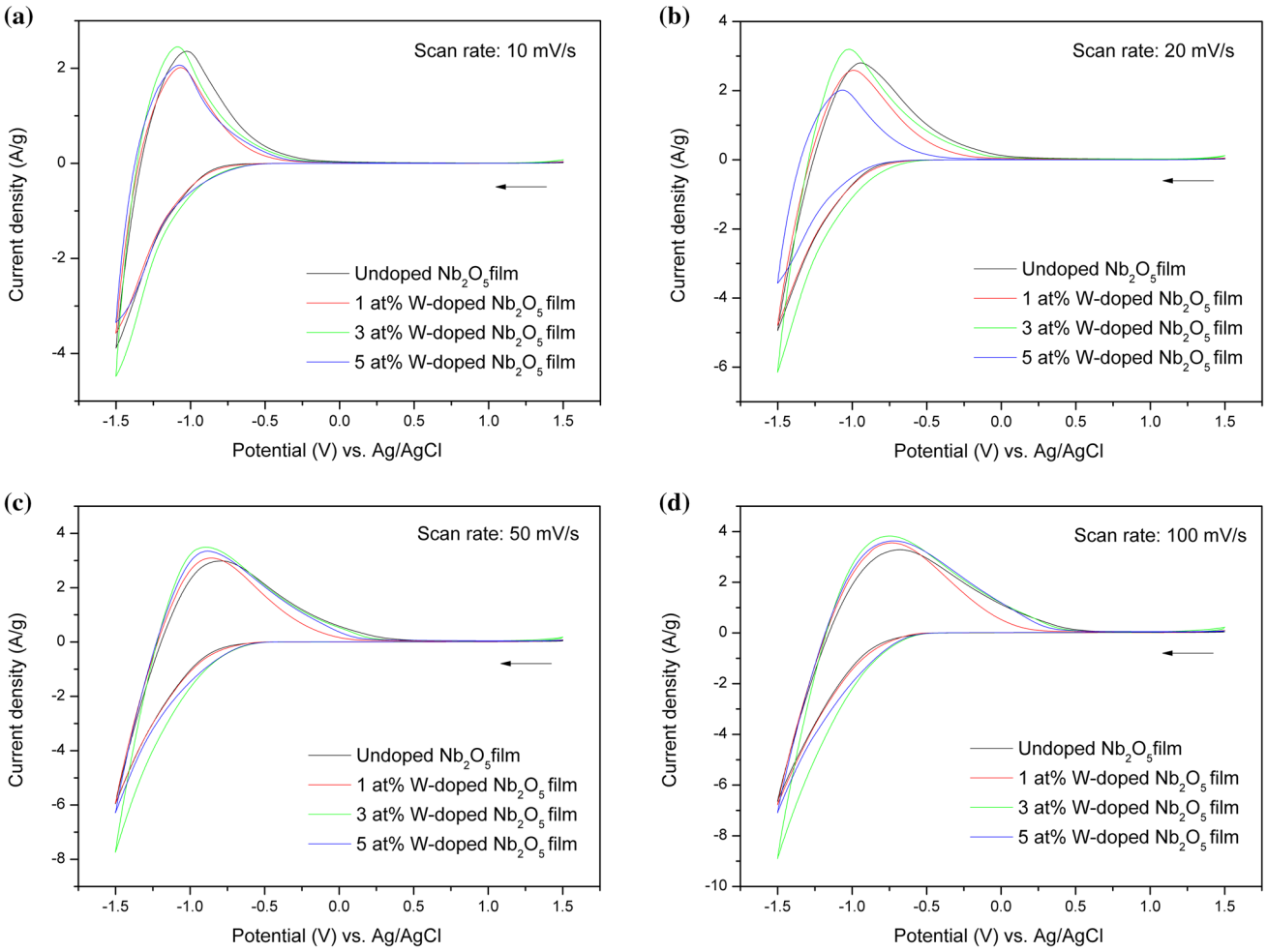

Fig. 7 **a–d** Cyclic voltammograms of the Nb_2O_5 thin films at different scan rates. Arrow indicates the scan direction

out using SEM micrographs, shown in Fig. 3a–d. The SEM micrograph of the undoped film reveals that the film has the porous and interlinked nano-fibrous morphology. Agglomeration of nano-fibres at a few places is also observed. Upon 1 at.% W doping, the nano-fibrous morphology changes to a morphology comprising of irregular shaped large grains with agglomeration of grains at a few places. On increasing W doping to 3 at.%, the morphology appears to be denser with agglomeration of grains at relatively more places. Finally, with 5 at.% W doping, the morphology changes again to the short nano-fibrous morphology including the irregular shaped large grains at a few places. The EDS spectra of elemental analyses of the films are shown in Fig. 3e–h which confirms the presence of Nb and O in the undoped film, and W, Nb and O in the W-doped films.

The AFM images of the Nb_2O_5 films were recorded in non-contact mode, and the two-dimensional (2D) and three-dimensional (3D) topographic images of scan area (3 μm × 3 μm) are shown in Fig. 4a–h. The surface topographical parameters of the films have been determined using Nova AFM software and are listed in Table 2. Compared with the undoped film, the image surface area has been found to enhance in the 1 and 3 at.% W-doped films, but it decreases in the 5 at.% W-doped film. It is obvious from Table 2 that the 3 at.% W-doped film has the maximum root mean square (rms) roughness. Usually, higher is the rms roughness of the film, larger would be the image surface area of the film and consequently the film would be more conducive to exhibit improved electrochromic performance.

3.3 Optical studies

Figure 5 presents the transmission spectra of the undoped and W-doped Nb_2O_5 thin films deposited on plane glass substrates. Undoped Nb_2O_5 film exhibits optical transmittance varying between 60% and 65% in the visible range. Upon W doping, the transmittance deceases first for the 1 at.% doping and then increases again for the 3 at.% and

Table 3 Analyses of cyclic voltammetry measurements of the undoped and W-doped Nb_2O_5 thin films

Samples	Scan rate (mV/s)	Cathodic peak current density, J_{pc} (A/cm^2)	Cathodic peak potential, V_{pc} (V)	Anodic peak current density, J_{pa} (A/cm^2)	Anodic peak potential, V_{pa} (V)	Diffusion coefficient (cm^2/s)		Charge intercalated (C/g)	Charge deintercalated (C/g)	Reversibility (%)	Colouration efficiency at 600 nm (cm^2/C)
						$D_{insertion}$	$D_{extraction}$				
Undoped Nb_2O_5 film	10	7.78E−04	− 1.50	4.71E−04	− 1.02	8.17E−12	3.00E−12	131.32	122.96	93.63	24.7
	20	9.88E−04	− 1.50	5.60E−04	− 0.94	6.60E−12	2.12E−12	92.59	86.82	93.76	
	50	1.19E−03	− 1.50	5.97E−04	− 0.79	3.83E−12	9.62E−13	50.84	47.73	93.89	
	100	1.33E−03	− 1.50	6.56E−04	− 0.69	2.38E−12	5.82E−13	30.97	29.58	95.52	
1 at.% W-doped Nb_2O_5 film	10	7.14E−04	− 1.50	4.03E−4	− 1.07	6.90E−12	2.19E−12	121.14	93.40	83.46	37.4
	20	9.58E−04	− 1.50	5.18E−4	− 0.99	6.20E−12	1.81E−12	88.43	69.06	93.66	
	50	1.19E−03	− 1.50	6.18E−4	− 0.86	3.81E−12	1.03E−12	50.13	42.02	89.87	
	100	1.36E−03	− 1.50	7.10E−4	0.73	2.48E−12	6.82E−13	31.28	27.63	86.77	
3 at.% W-doped Nb_2O_5 film	10	7.17E−04	− 1.50	3.92E−04	− 1.09	6.95E−12	2.08E−12	152.02	119.12	78.36	68.7
	20	9.84E−04	− 1.50	5.11E−04	− 1.02	6.54E−12	1.77E−12	115.02	90.58	78.75	
	50	1.24E−03	− 1.50	5.59E−04	− 0.89	4.15E−12	8.44E−13	67.18	53.66	79.87	
	100	1.42E−03	− 1.50	6.12E−4	− 0.75	2.74E−12	5.06E−13	42.51	34.19	80.42	
5 at.% W-doped Nb_2O_5 film	10	6.69E−04	− 1.50	4.13E−4	− 1.08	6.05E−12	2.31E−12	121.46	101.76	83.78	40.4
	20	9.81E−04	− 1.50	5.74E−4	− 0.99	6.50E−12	2.22E−12	92.53	79.60	86.03	
	50	1.26E−03	− 1.50	6.69E−4	− 0.88	4.27E−12	1.21E−12	55.10	50.04	90.82	
	100	1.42E−03	− 1.50	7.26E−4	− 0.72	2.72E−12	7.12E−13	34.50	33.03	95.74	

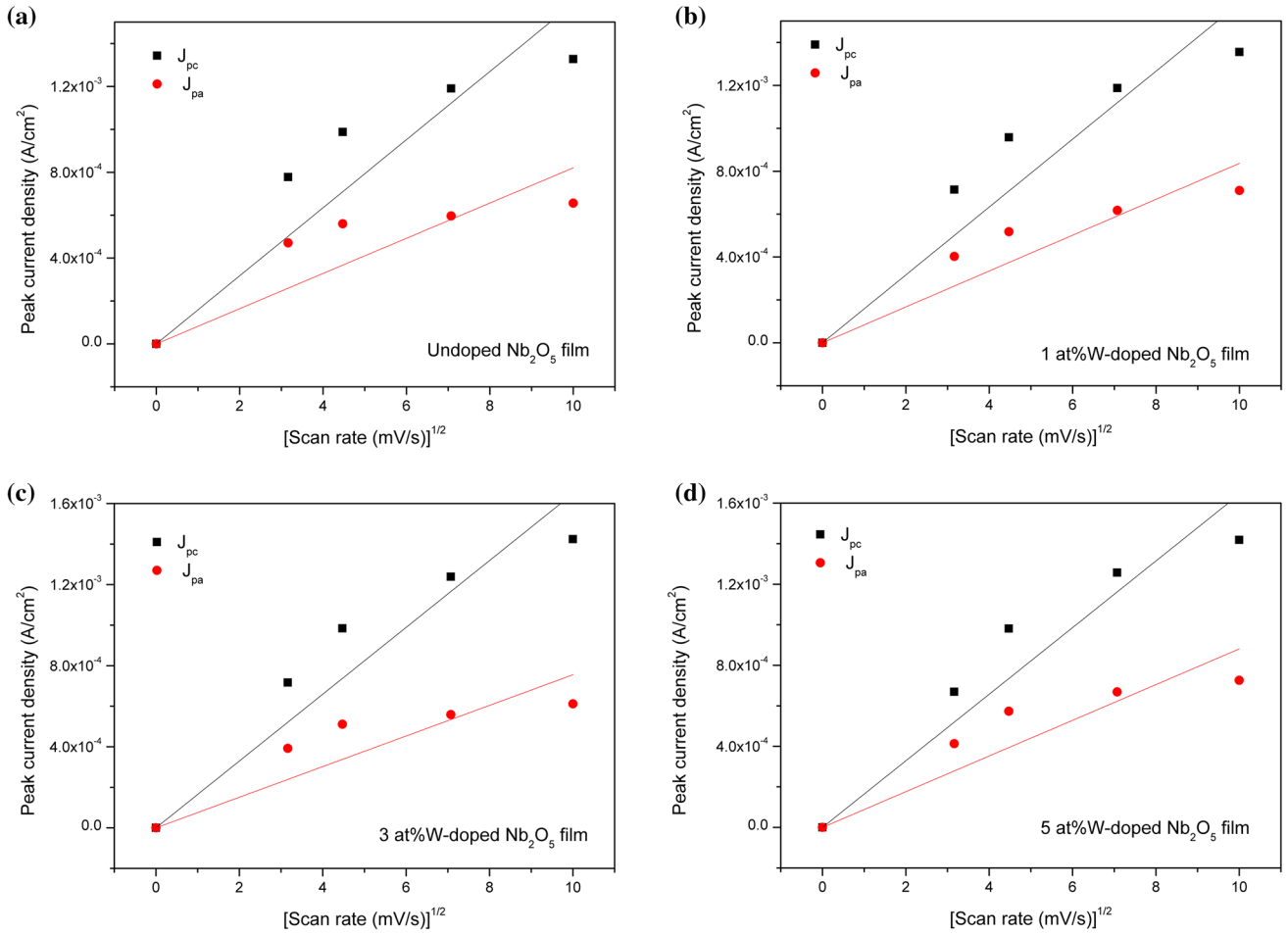

Fig. 8 **a–d** Plots of peak current densities versus the square root of potential scan rates

5 at.% doped films relative to the undoped film. Variation in transmittance is attributed to the scattering of light owing to different film morphologies (surface roughness) [21, 22].

Both direct and indirect energy band gap transitions in Nb_2O_5 have been reported in literatures [6, 7, 13, 23]. The energy band gaps for direct and indirect transitions can be obtained employing the Tauc method [22] by extrapolating the linear portion of a plot of $(Ah\nu)^2$ versus $h\nu$ for direct transition, or $(Ah\nu)^{1/2}$ versus $h\nu$ for indirect transition, to the abscissa, where A is the optical absorbance, and $h\nu$ is the photon energy. Figure 6 presents the required plot for direct transition in Nb_2O_5 films. The energy bandgap values thus obtained are found to be ~ 3.60 eV. Upon 1 at.% W doping, a little change in the energy bandgap value is observed, which may be attributed to the density of localized energy states in the bandgap. It has been reported that the energy bandgap values vary in the range of 3.2–3.9 eV for Nb_2O_5 films prepared by different techniques [24] (and references therein).

3.4 Electrochromic studies

3.4.1 Cyclic voltammetry

Cyclic voltammetry (CV) measurements were performed by applying dc potential sweep in the range of ± 1.5 V (vs. Ag/AgCl reference electrode) at four different potential scan rates 10, 20, 50 and 100 mV/s in the 0.1 M $LiClO_4$/propylene carbonate electrolyte. The cyclic voltammograms of the films comprising of a single oxidation–reduction cycle are depicted in Fig. 7a–d. It has been found that during cathodic scan the Nb_2O_5 film electrodes undergo a progressive increase in the blue coloration under the application of increasing negative potential, whereas during anodic scan the blue film electrodes become bleached and colourless when they are subjected to positive potential. During cathodic scan, on the application of increasing negative potential, the negative current density begins to increase, attaining a highest value when the film gets maximum blue coloration. Blue colouration to the film arises due to insertion of electrons and Li^+ ions into the Nb_2O_5 films, which causes reduction of Nb^{5+} ions to lower valence state

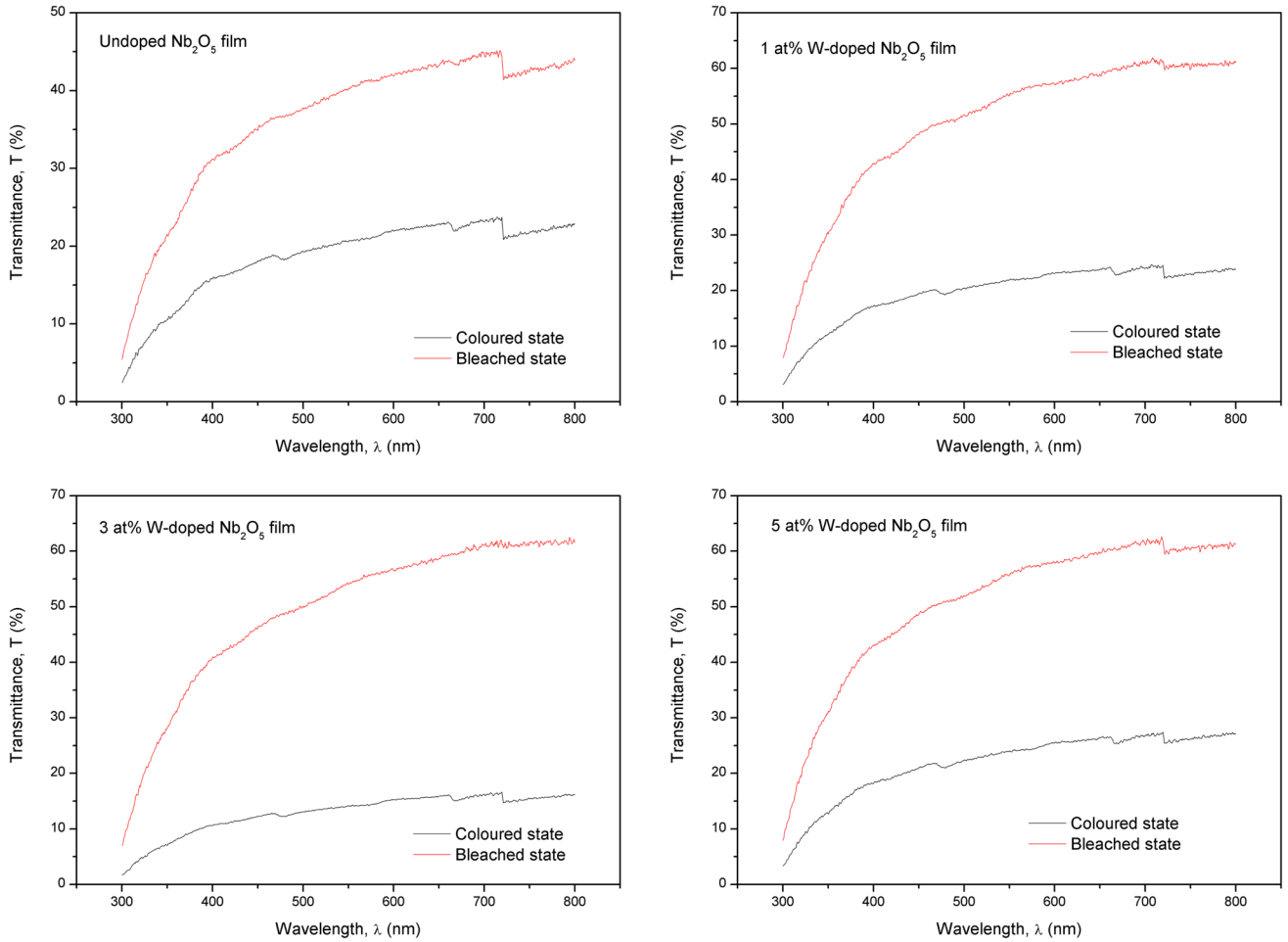

Fig. 9 Transmittance spectra of the Nb_2O_5 films in coloured and bleached states

Nb^{4+} ions. For anodic scan, when the potential changes from − 1.5 to + 1.5 V, the current density begins to change from negative to positive value, attaining a highest value and then decreases during which the film is bleached. This phenomenon occurs due to intercalated charge extraction from the film structure; consequently, Nb^{4+} ions get oxidised to Nb^{5+} ions, resulting in the bleaching of film. Coloration and bleaching phenomena in Nb_2O_5 films can be represented by the following electrochemical redox reaction [13]:

$$Nb_2O_5(\text{colourless}) + xLi^+ + xe^- \leftrightarrow Li_xNb_2O_5(\text{blue}) \quad (5)$$

$Li_xNb_2O_5$ is, in general, called as the lithium-niobium bronze. The cathodic and anodic peak current densities and the corresponding cathodic and anodic potentials at different scan rates for all the films are listed in Table 3. Charges intercalated and deintercalated during cathodic scan and anodic scan, respectively have been obtained from the integration of respective parts of cyclic voltammograms, and are listed in Table 3. As evident from Table 3, the net charge density for the films improves upon W doping. In the case of 10 mV/s scan rate, the net charge density for the undoped Nb_2O_5 thin film has been found to be 8.4 C/g, whereas for the same scan rate, the net charge densities have been obtained to be 27.7 C/g, 32.9 C/g, and 19.7 C/g for the 1, 3 and 5 at.% W-doped films, respectively. Further, in each film, the net charge density has been observed to decrease with the increasing scan rate. This may be attributed to the fact that at higher scan rates the Li^+ ions do not get enough time to intercalate/deintercalate into and out the film.

All the cyclic voltammograms exhibit a spike at the potential of − 1.5 V during cathodic scan and a peak during anodic scan. Non-appearance of a well-defined peak in cathodic region is a consequence of the formation of back emf within the niobium bronze during ion insertion. Figure 8a–d shows the linear variation of cathodic/anodic peak current densities with the square root of the potential scan rates, which confirms a diffusion controlled mechanism in the redox reaction process.

In each film, the cathodic and anodic peak current densities have been found to enhance with the increase in scan

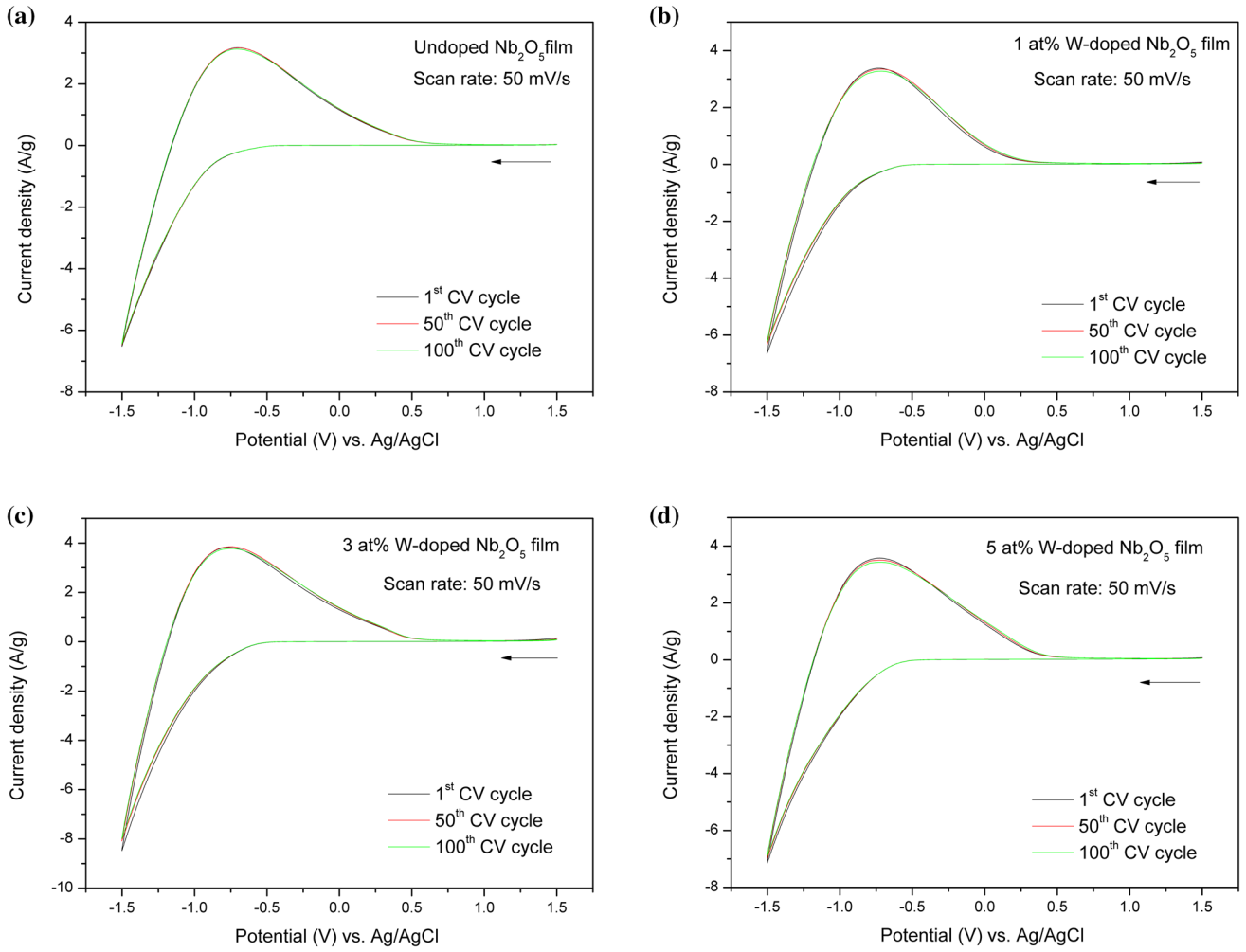

Fig. 10 **a–d** Electrochemical stability of the Nb_2O_5 films

rates. This is attributed to the fact that on increasing the potential scan rate, the diffusion layer at the film electrode surface gets shortened, and consequently an increase in the current density is observed. It is also noticed that the anodic peak current position shifts with the varying scan rate. Changing of anodic peak position towards higher potential implies that the change from coloured to bleached state is slower [25]. This may be attributed to decrease in the rate of bleaching kinetics and residual coloration. Further, relative to the undoped Nb_2O_5 film, the anodic peak current position shifts towards the lower potential in the W-doped films. This implies that the rate of bleaching kinetics is faster in the W-doped Nb_2O_5 films, which is closely linked to the microstructural characteristics of the films.

The diffusion coefficient of Li^+ ions into the Nb_2O_5 host lattice has been determined using the Randles–Sevcik equation [26]:

$$D^{1/2} = \frac{J_p}{2.72 \times 10^5 n^{3/2} C \nu^{1/2}} \tag{6}$$

where D is the diffusion coefficient (cm^2/s), J_p is the peak current density (A/cm^2), n is the number of electrons involved in the redox process (it is assumed to be 1), C is the concentration of active ions in the electrolyte solution (mol/cm^3), and ν is the scan rate (V/s). A change in the diffusion coefficient value upon W doping is attributed to varying mobility of the diffusing ionic species (Li^+) in the redox reaction. In fact, microstructural characteristics of the film affect mobility of the diffusing ionic species to a great extent.

Colouration efficiency (η) is a wavelength-dependent electrochromic parameter correlating the optical contrast with the charges intercalated per unit electrode area, defined by the relation [27]:

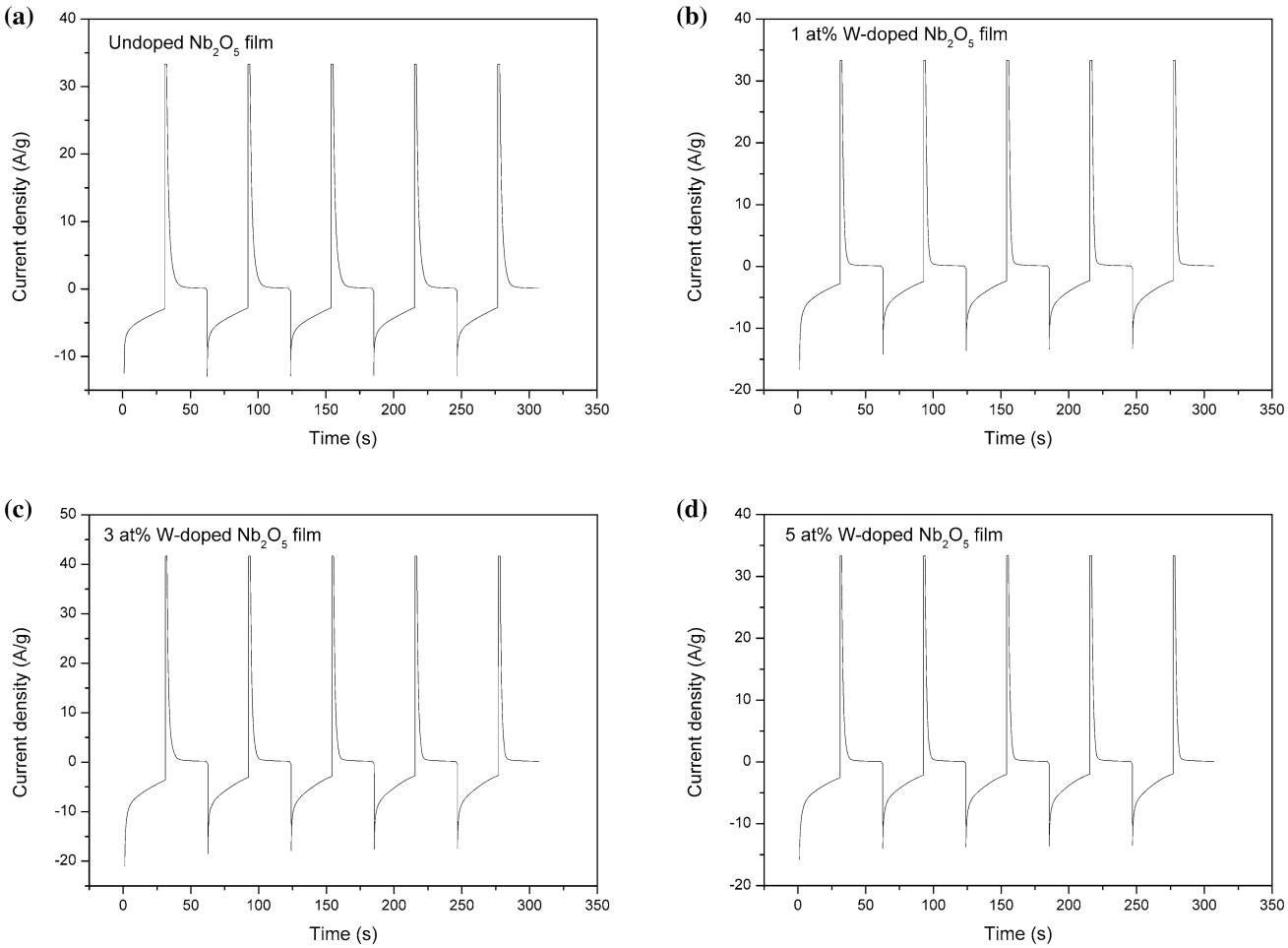

Fig. 11 **a–d** Chronoamperometry curves of the undoped and W-doped Nb_2O_5 thin films

Table 4 Analyses of chronoamperometry measurements of the undoped and W-doped Nb_2O_5 thin films

Samples	Charge intercalated (C/g)	Charge extracted (C/g)	Reversibility (%)	Colouration time (s)	Bleaching time (s)
Undoped Nb_2O_5 film	136.54	109.70	80.3	> 30	4.1
1 at.% W-doped Nb_2O_5 film	143.77	87.77	61.1	24.1	3.2
3 at.% W-doped Nb_2O_5 film	173.23	113.25	65.4	25.3	3.5
5 at.% W-doped Nb_2O_5 film	141.49	80.64	57	23.7	3.0

$$\eta(\lambda) = \frac{\Delta OD}{Q/A} = \frac{\ln\left(T_{bleached}/T_{coloured}\right)}{Q/A} \quad (7)$$

where ΔOD is the change in optical density, $T_{coloured}$ and $T_{bleached}$ are the transmittances of the film in coloured and bleached states, respectively at a certain wavelength, Q is the intercalated charge, and A is the film electrode area. Figure 9 presents the transmittance spectra of the films in coloured and bleached states. It is evident from Fig. 9 that the 3 at.% W-doped film has the maximum optical density. The colouration efficiency of the Nb_2O_5 film has been found to improve upon W doping with the optimum value 68.7 cm^2/C at 600 nm for the 3 at.% W-doped Nb_2O_5 film.

To examine the electrochemical stability of the Nb_2O_5 films, reduction–oxidation cycles were repeated several

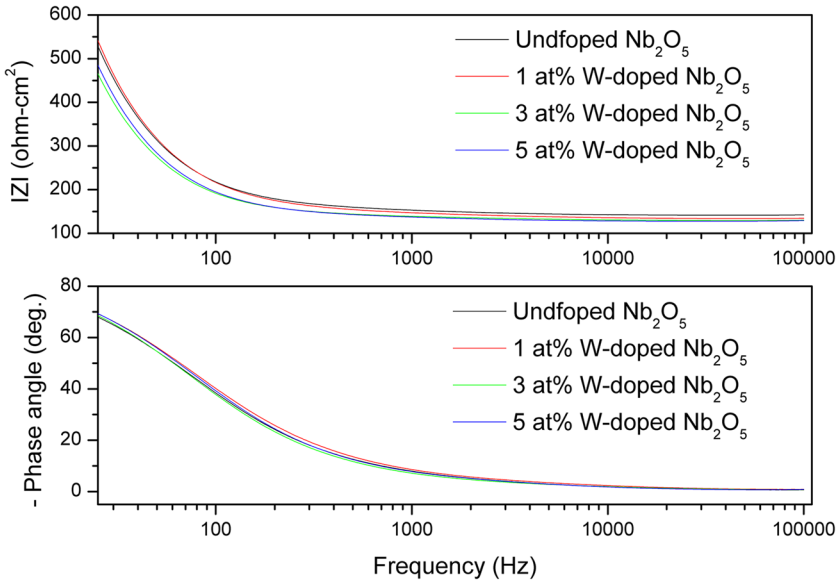

Fig. 12 Bode magnitude/phase angle plots of the Nb_2O_5 films

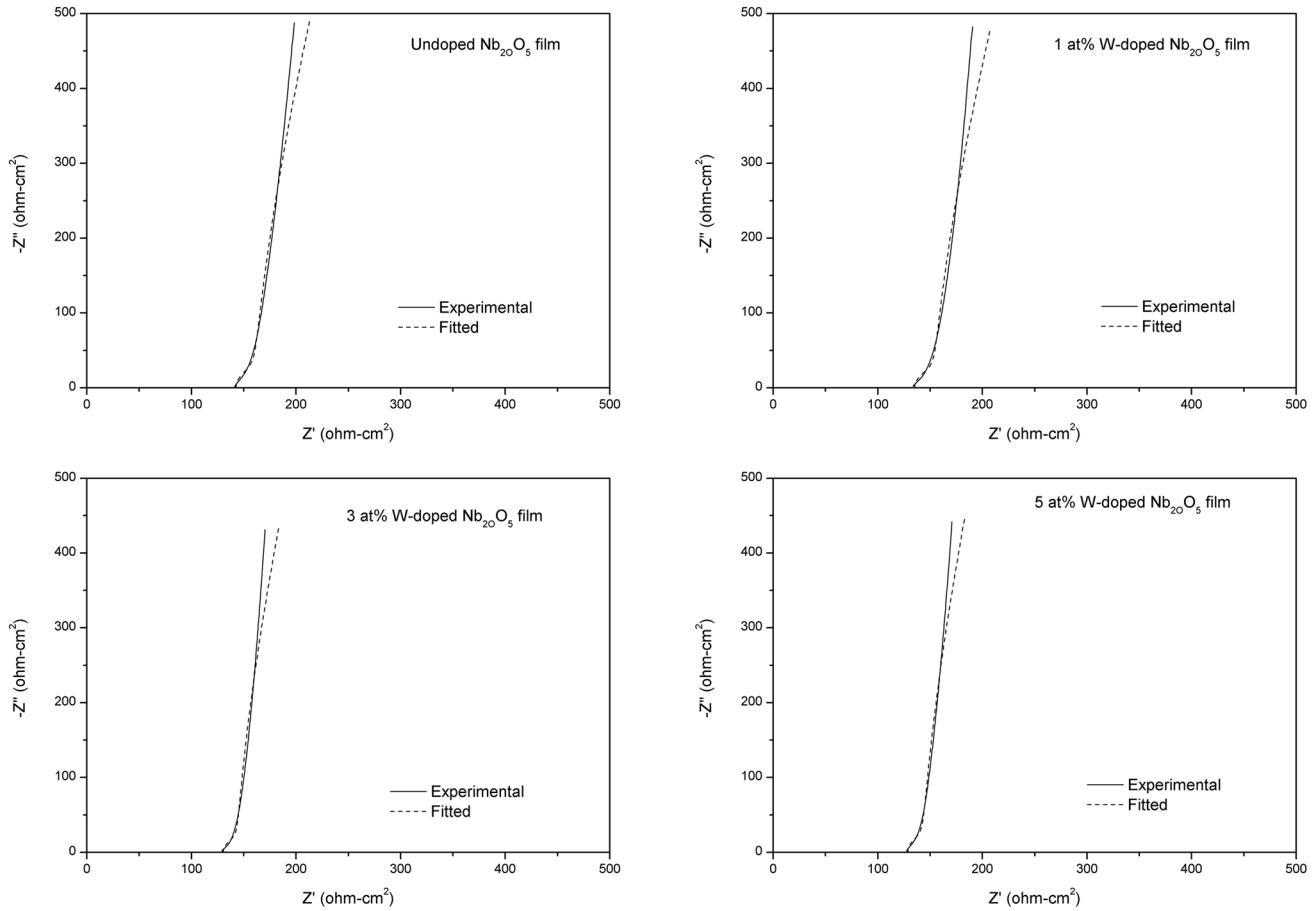

Fig. 13 Nyquist impedance plots of the Nb_2O_5 films

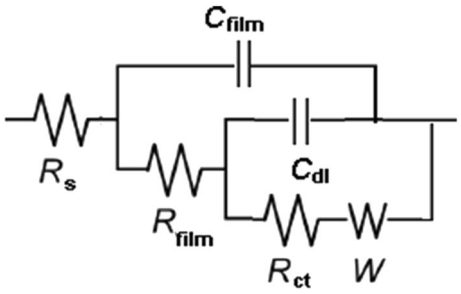

Fig. 14 Equivalent electrical circuit used for fitting the EIS experimental data

times by applying a dc potential sweep in the range of ± 1.5 V (vs. Ag/AgCl reference electrode) (Fig. 10a–d). It is clear from Fig. 10a–d that in each case the cyclovoltammetric curve remains almost unchanged even after 100 reduction–oxidation cycles, which establishes excellent electrochemical stability of the films.

3.4.2 Chronoamperometry

Figure 11a–d shows chronoamperometric plots of the Nb_2O_5 films, which were recorded for 30 s by applying a dc potential stepped between –1.5 V and +1.5 V (vs. Ag/AgCl reference electrode) for 5 cycles. During the time interval 0–30 s, the film was in colored state on stepping the voltage from its initial potential of 0.0 to − 1.5 V for 30 s, while during the next time interval 30–60 s the film was in bleached state on reversing the voltage to +1.5 V. As evident from Fig. 11a–d, both coloration current density and bleaching current density following the potential step are smooth and decrease continuously with time. It is obvious from Table 4 that the reversibility of the film decreases upon W doping. The colouration and bleaching times have been estimated from the current versus time transients. It has been found that the colouration and bleaching times of the film upon W doping become short relative to the undoped film, and therefore the switching response of the film improves upon W doping. In general, the coloration process is slower than the bleaching in both undoped and W-doped Nb_2O_5 films due to faster bleaching kinetics [28].

3.4.3 Electrical impedance spectroscopy

Figure 12 presents the Bode plots representing the impedance (Z) and the phase angle of the Nb_2O_5 films as a function of frequency. It shows the frequency domain behavior of the system. As evident from Fig. 12, the phase angle at a certain frequency remains almost the same for all the films, but relative to the undoped film, the impedance shows a little variation upon W doping. For all the films, the impedance has been found to be maximum at the lowest frequency and decreases exponentially with the increase of frequency of ac signal. This is attributed to the fact that the interface energy states near the grain boundaries in the film response effectively at lower frequencies of ac signal owing to their large relaxation times.

Plots of the real versus imaginary components of the impedance of the Nb_2O_5 films measured in the frequency range of 100 kHz–24 Hz are depicted in Fig. 13, and are referred to as the Nyquist impedance plots. These plots have been characterized using Nova software by means of fit and simulation analysis. The equivalent electrical circuit, shown in Fig. 14, has been used for fitting the EIS data, and the circuit fitting parameters are listed in Table 5. The lower values of goodness of fit, χ^2, for the fitting curves indicate that the proposed EEC model is in good agreement with the experimental data. In the EEC, R_s is the resistance of $LiClO_4$/propylene carbonate electrolyte; R_{film} and C_{film} are the Nb_2O_5 film resistance and capacitance, respectively; R_{ct} is the charge transfer resistance (interfacial reaction resistance); W is the Warburg diffusion impedance (ionic diffusion in the film electrode), and C_{dl} is the double-layer capacitance of the Nb_2O_5/electrolyte interface [29]. Mathematically, Warburg impedance is described as: $W = 1/[Y_0 (j\omega)^{0.5}]$, where Y_0 is the admittance ($1/|Z|$) at $\omega = 1$ rad/s. It is inferred from Table 5 that the circuit elements are strongly dependent upon the microstructural features of the films. The varying charge transfer resistances are attributed to the fact that effective surface areas of the films in contact with the electrolyte and the redox reaction rates at different locations over the film surface are different.

A comparison of electrochromic performance of W-doped Nb_2O_5 films (this work) with those of other Nb_2O_5-based films reported earlier in literatures is presented in Table 6.

Table 5 Electrical parameters resulting from the fitting of the experimental data to the EEC

Samples	R_S (Ω-cm^2)	C_{film} (μF/cm^2)	R_{film} (Ω-cm^2)	R_{ct} (μΩ-cm^2)	$\frac{W(\Omega\ cm^2\ s^{0.5})}{Y_o(\mu\Omega^{-1}\ cm^{-2})}$	C_{dl} (μF/cm^2)	χ^2
Undoped Nb_2O_5 film	142	4.95	54.8	21.9	23.4	6.56	0.0499
1 at.% W-doped Nb_2O_5 film	135	4.31	50.0	15.9	24.3	6.72	0.0866
3 at.% W-doped Nb_2O_5 film	130	5.42	38.3	13.3	22.8	7.81	0.0586
5 at.% W-doped Nb_2O_5 film	128	5.59	46.3	14.4	21.4	7.09	0.0411

Table 6 Electrochromic performance of Nb_2O_5-based thin films prepared by various methods

MoO_3-based films	Deposition/preparation method	Electrochromic performance	References
Ta_2O_5-doped Nb_2O_5 films	Sol–gel spin-coating	The films have the charge density of 5 mC/cm^2 and exhibit good kinetics in CV measurements.	[6]
Nanostructured Nb_2O_5 films	Sol–gel spin-coating	The Nb_2O_5 films annealed at 500 °C have the optical modulation 30.6% and the coloration efficiency 25 cm^2/C (at 500 nm).	[7]
Nb_2O_5:Ti films Nb_2O_5:Mo films	Sol–gel dip-coating	The Nb_2O_5:Ti films sintered at 600 °C have the coloration efficiency 27 cm^2/C whereas the Nb_2O_5:Mo films sintered at 500 °C exhibit the coloration efficiency 21.5 cm^2/C at 500 nm wavelength	[9]
WO_3-doped Nb_2O_5 films	Sol–gel dip coating	The 5% WO_3-doped Nb_2O_5 films have the fast insertion/extraction kinetics for Li^+/H^+ ions.	[11]
Nb_2O_5 films	Spray pyrolysis technique	The spray-deposited Nb_2O_5 films exhibit the coloration efficiency 13 cm^2/C and the reversibility 85%, which decrease on annealing the films.	[13]
Nb_2O_5 films	Chemical vapour deposition	The Nb_2O_5 films prepared at 350 °C have the coloration efficiency of 160 cm^2/C at 550 nm wavelength.	[14]
Nb_2O_5 nanorod array films	Hydrothermal process	The Nb_2O_5 nanorods films have a high specific capacity of about 380 mAh/g	[15]
Nb_2O_5:MoO_3 thin films	RF magnetron sputtering	The Nb_2O_5:MoO_3 (85:15) films show the optimum coloration efficiency of 2.303 mm^2/C at 633 nm.	[23]
WO_3–Nb_2O_5 composite films	Fast-alternating bipolar-pulsed magnetron sputtering	The WO_3–Nb_2O_5 composite films can sustain over 3×10^4 reduction–oxidation cycles with transmission modulations above 20%.	[30]
Anodized nanoporous Nb_2O_5 films	RF sputtering and electrochemical anodization	The anodized Nb_2O_5 films have the coloration efficiency 47 cm^2/C at 550 nm	[31]
Nb_2O_5 films	Sol–gel technique	The solution-processed Nb_2O_5 films coupled with p-type electrochromic polymers show a high contrast, fast switching time, high coloration efficiency and stable cycling performance	[32]
W-doped Nb_2O_5 films	Sol–gel dip-coating	The 3 at.% W-doped films exhibit the excellent electrochemical stability and the optimum coloration efficiency 68.7 cm^2/C at 600 nm	This work

4 Conclusions

(a) Nb_2O_5 thin films (undoped and W-doped) prepared by the dip-coating process using sols obtained by the chloroalkoxide route are polycrystalline possessing an orthorhombic phase of niobium pentaoxide.
(b) Undoped and the film doped with 5 at.% W have the nano-fibrous morphology, whereas 1 at.% and 3 at.% W-doped films have a morphology comprising of irregular shaped large grains.
(c) Roughness factor defined as the ratio of the image surface area to the image projected surface area is in the range 1.32–4.31 for these films.
(d) The 3 at.% W-doped film exhibits the best coloration efficiency 68.7 cm^2/C at 600 nm.
(e) All the films show excellent electrochemical stability, and the switching response of the film improves upon W doping.

Acknowledgements The use of XRD and UV–Vis measurement facilities at Centre for Interdisciplinary Research, MNNIT Allahabad, India, and FESEM and SPM characterization facilities at Central Instrument Facility, IIT BHU, Varanasi, India are gratefully acknowledged. Financial support provided under the project, Third phase of Technical Education Quality Improvement Programme (referred to as TEQIP-III), Ministry of Human Resource Development, Govt. of India is also appreciatively acknowledged.

References

1. P. Ashrit, in *Transition Metal Oxide Thin Film–Based Chromogenics and Devices*, Elsevier Metal Oxide Series, ed. by G. Korotcenkov (Elsevier, Cambridge, United States, 2017)
2. M.A. Aegerter, Sol–gel chromogenic materials and devices, in *Structure and Bonding: Optical and Electronic Phenomena in Sol-Gel Glasses and Modern Applications*, vol. 85, ed. by R. Reisfeld, C. Jorgensen (Springer, Berlin, 1996), pp. 149–194
3. M.A. Aegerter, M. Schmitt, Y. Guo, Sol–gel niobium pentoxide coatings: applications to photovoltaic energy conversion and electrochromism. Int. J. Photoenergy **4**, 1–10 (2002)
4. J. He, H. Yongming, Z. Wang, L. Wei, S. Yang, W. Guitai, Yu. Wang, S. Wang, G. Haoshuang, J. Wang, Hydrothermal growth and optical properties of Nb_2O_5 nanorod arrays. J. Mater. Chem. C **2**, 8185 (2014)
5. J.K. Dash, L. Chen, M.R. Topka, P.H. Dinolfo, L.H. Zhang, K. Kisslinger, T.-M. Lua, G.-C. Wang, A simple growth method for Nb_2O_5 films and their optical properties. RSC Adv. **5**, 36129 (2015)
6. E. Pehlivan, K. Koc, F.Z. Tepehan, G.G. Tepehan, Structural, optical and electrochromic properties of tantalum pentoxide-doped niobium pentoxide thin films. J. Sol Gel Sci. Technol. **77**, 172 (2016)
7. A. Verma, P.K. Singh, Sol–gel derived nanostructured niobium pentoxide thin films for electrochromic applications. Ind. J. Chem. **52A**, 593 (2013)
8. A. Pawlicka, M. Atik, M.A. Aegerter, Synthesis of multicolor Nb_2O_5 coatings for electrochromic devices. Thin Solid Films **301**, 236 (1997)
9. M. Schmitt, M.A. Aegerter, Electrochromic properties of pure and doped Nb_2O_5 coatings and devices. Electrochim. Acta **46**, 2105 (2001)
10. S. Heusing, D.-L. Sun, J. Otero-Anaya, M.A. Aegerter, Grey, brown and blue coloring sol–gel electrochromic devices. Thin Solid Films **502**, 240 (2006)
11. E. Pehlivan, F.Z. Tepehan, G.G. Tepehan, Comparison of optical, structural and electrochromic properties of undoped and WO_3-doped Nb_2O_5 thin films. Solid State Ionics **165**, 105 (2003)
12. A.M. Al-Baradi, M.M. El-Nahass, A.M. Hassanien, A.A. Atta, M.S. Alqahtani, A.O. Aldawsari, Influence of RF sputtering power on structural and optical properties of Nb_2O_5 thin films. Optik **168**, 853 (2018)
13. S.H. Mujawar, A.I. Inamdar, C.A. Betty, V. Ganesan, P.S. Patil, Effect of post annealing treatment on electrochromic properties of spray deposited niobium oxide thin films. Electrochim. Acta **52**, 4899 (2007)
14. T. Maruyama, T. Kanagawa, Electrochromic properties of niobium oxide thin films prepared by chemical vapor deposition. J. Electrochem. Soc. **141**, 2868 (1994)
15. H. Wen, Z. Liu, J. Wang, Q. Yang, Y. Li, Yu. Jerry, Facile synthesis of Nb_2O_5 nanorod array films and their electrochemical properties. Appl. Surf. Sci. **257**, 10084 (2011)
16. X. Tang, X. Yan, Dip-coating for fibrous materials: mechanism, methods and applications. J. Sol Gel Sci. Technol. **81**, 378 (2017)
17. C.J. Brinker, G.W. Scherer, *Sol-Gel Science: The Physics and Chemistry of Sol-Gel Processing* (Academic Press, Boston, 2013)
18. N. Ozer, D.-G. Chen, C.M. Lampert, Preparation and properties of spin-coated Nb_2O_5 films by the sol–gel process for electrochromic applications. Thin Solid Films **277**, 162 (1996)
19. N. Ozer, M.D. Rubin, C.M. Lampert, Optical and electrochemical characteristics of niobium oxide films prepared by sol-gel process and magnetron sputtering: a comparison. Sol. Energy Mater. Sol. Cells **40**, 285 (1996)
20. A.M. Raba, J. Bautista-Ruíz, M.R. Joy, Synthesis and structural properties of niobium pentoxide powders: a comparative study of the growth process. Mater. Res. **19**, 1381 (2016)
21. D. Beena, K.J. Lethy, R. Vinodkumar, V.P.M. Pillai, V. Ganesan, D.M. Phase, S.K. Sudheer, Effect of substrate temperature on structural, optical and electrical properties of pulsed laser ablated nanostructured indium oxide films. Appl. Surf. Sci. **255**, 8334 (2009)
22. A. Goswami, *Thin Film Fundamentals* (New Age International (P) Ltd., New Delhi, 2005)
23. N. Usha, R. Sivakumar, C. Sanjeeviraja, Structural, optical and electrochromic properties of Nb_2O_5:MoO_3 (95:5, 90:10, and 85:15) thin films prepared by RF magnetron sputtering technique. Mater. Lett. **229**, 189 (2018)
24. C.G. Granqvist, *Handbook of Inorganic Electrochromic Materials* (Elsevier, Amsterdam, 2002)
25. J.M. O-Rueda de León, D.R. Acosta, U. Pal, L. Castañeda, Improving electrochromic behavior of spray pyrolised WO_3 thin solid films by Mo doping. Electrochim. Acta **56**, 2599 (2011)
26. R. Mukherjee, P.P. Sahay, Improved electrochromic performance in sprayed WO_3 thin films upon Sb doping. J. Alloys Compd. **660**, 336 (2016)
27. A. Kumar, C.S. Prajapati, P.P. Sahay, Modification in the microstructural and electrochromic properties of spray-pyrolysed WO_3 thin films upon Mo doping. J. Sol Gel Sci. Technol. **90**, 281 (2019)
28. S.R. Bathe, P.S. Patil, Influence of Nb doping on the electrochromic properties of WO_3 films. J. Phys. D Appl. Phys. **40**, 7423 (2007)
29. S.H. Lee, H.M. Cheong, C.E. Tracy, A. Mascarenhas, J.R. Pitts, G. Jorgensen, S.K. Deb, Alternating current impedance and Raman spectroscopic study on electrochromic a-WO_3 films. Appl. Phys. Lett. **76**, 3908 (2000)
30. C.-J. Tang, J.-L. He, C.-C. Jaing, C.-J. Liang, C.-H. Chou, C.-Y. Han, C.-L. Tien, An all-solid-state electrochromic device based on WO_3–Nb_2O_5 composite films prepared by fast-alternating bipolar-pulsed reactive magnetron sputtering. Coatings **9**, 9 (2019)
31. D.D. Yao, R.A. Rani, A.P. O'Mullane, K. Kalantar-zadeh, J.Z. Ou, High performance electrochromic devices based on anodized nanoporous Nb_2O_5. J. Phys. Chem. C **118**, 476 (2014)
32. J. He, L. You, D.T. Tran, J. Mei, Low-temperature thermally-annealed niobium oxide thin films as a minimally color changing ion storage layer in solution-processed polymer electrochromic devices. ACS Appl. Mater. Interfaces **11**, 4169 (2019)